Inorganic Chemistry

Article

pubs.acs.org/IC

Concerted Proton–Electron Transfer in Electrocatalytic O_2 Reduction by Iron Porphyrin Complexes: Axial Ligands Tuning H/D Isotope Effect

Sudipta Chatterjee, Kushal Sengupta, Subhra Samanta, Pradip Kumar Das, and Abhishek Dey*

Department of Inorganic Chemistry, Indian Association for the Cultivation of Science, Kolkata 700032, India

Supporting Information

ABSTRACT: The electrochemical O_2 reduction by thiolate- and imidazole-bound iron porphyrin complexes and H/D isotope effects on $4e^-$ (determined by rotating disc electrochemistry) and $2e^-$ (determined by rotating ring disc electrochemistry) O_2 reduction rates are investigated. The results indicate that a thiolate axial ligand shows an H/D isotope effect greater than 18 and 47 for the $4e^-$ and $2e^-$ O_2 reductions, respectively. Alternatively, an imidazole axial ligand results in H/D isotope effects of 1.04 and 4.7 for the $4e^-$ and $2e^-$ O_2 reduction, respectively. The catalytic O_2 reduction mechanism is investigated in situ with resonance Raman coupled with rotating disc electrochemistry. The data indicate that the rate-determining step changes from O–O bond heterolysis of Fe^{III}–OOH species for a thiolate axial ligand to an O–O bond heterolysis of an Fe^{II}–OOH for an imidazole axial ligand.

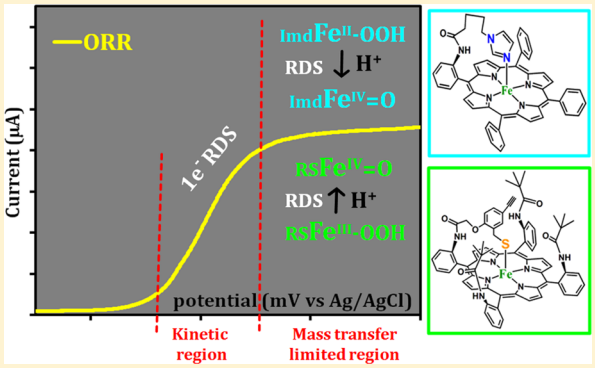

INTRODUCTION

Involvement of concerted proton–electron transfer or proton-coupled electron transfer (CPET/PCET) steps in the biological reduction and activation of O_2 has long been established.[1−8] The importance of CPET steps in proton pumping across the mitochondrial membrane during oxidative phosphorylation provides a compelling motivation for detailed understanding of this phenomenon.[9] The formal Born–Oppenheimer approximation, which allows the proton and electron coordinates to be separately treated due to large differences in their masses,[10,11] fails during a CPET process where the proton and electron movements are concerted and one has to treat the proton as a quantum entity that can tunnel through finite barriers.[12−14] Logically deuterium, a heavier isotope of proton, having smaller tunneling radius, can show much slower tunneling efficiencies, resulting in enormous H/D isotope effects for these elementary steps.[12,14−17] In nature, apart from cytochrome *c* oxidase (CcO),[4] CPET/PCET is also established to be involved to determine the thermodynamics and kinetics of reactions catalyzed by key transition metal active sites,[18,19] for example, superoxide dismutases, galactose oxidase, methane monooxygenase, riboneucleotide reductase, cytochrome P450 (cyt P450), photosystem II, and hydrogenases.[20−32]

Considering its importance in key biochemical pathways involved in nature, CPET has been widely investigated in synthetic inorganic systems.[33−47] Several milestones have been achieved in understanding the rates and isotope effects of a CPET/PCET process.[16,48−55] Roles of preorganized donor–acceptor centers in catalysis have been investigated along with conventional proton transfer from solvent.[3,56,57] In case of CPET, the solvent kinetic isotope effect (KIE) is determined by the overlap between the vibrational wave functions of the donor and acceptor along with the electron-transfer matrix element. In the absence of any structural attributes that induce a favorable geometry for proton transfer, the solvent KIE should be positive (>1) and large as the distance between the donor and the acceptor in the transition state is likely to be large. In the recent past, Meyer's group has reported that a PCET from heteroatom X (X = N, S, P, etc.) shows large values of primary KIE where X–H bond cleavage is involved in the rate-determining step (RDS).[53,58,59] However, Fukuzumi and Nam's group has recently shown an inverse deuterium KIE on the oxidative C–H bond cleavage to be present in a proposed PCET step.[60] Alternatively, a very large KIE is often observed in some cases of oxygen activation and substrate oxidation where hydrogen atom transfer involving tunneling, instead of CPET, is proposed to be involved.[51,61,62] However, details of the CPET steps involved in multistep O_2 reduction and its dependence on catalyst architecture remains largely unexplored.[63,64]

Understanding the elementary steps involved in the activation and reduction of O_2 to H_2O is not only important for designing efficient catalysts for practical applications but also for understanding the CPET steps likely involved in the enzymatic active sites of CcO and cyt P450.[46,65−70] Recently, we reported an iron porphyrin molecule containing a hydrogen-bonding distal architecture that shows efficient O_2 reduction

Received: December 15, 2014
Published: February 19, 2015

DOI: 10.1021/ic5029959
Inorg. Chem. 2015, 54, 2383−2392

over a wide pH range.[45,71] The mechanism of O_2 reduction catalyzed by this Fe-porphyrin complex changes from a sequential proton transfer followed by electron transfer in an organic solution to a CPET in aqueous solutions.[46] In parallel, we reported attachment of thiolate-bound iron porphyrin complexes to electrodes that could catalytically hydroxylate inert C−H bonds using high-valent intermediates produced during the electrochemical reduction of molecular O_2 at pH 7 showing turnover numbers in excess of 200.[72] In this manuscript we use a combination of electrochemistry and surface-enhanced resonance Raman spectroscopy coupled with rotating disc electrochemistry (SERRS-RDE)[73] to show how the mechanism of electrocatalytic reduction of O_2 by Fe-porphyrin complexes intrinsically depends on the nature of axial ligands (e.g., thiolate present in the above-mentioned functional mimic of cyt P450 and imidazole present in the functional mimics of CcO/Hb). Our findings indicate that, in an aqueous medium, while the thiolate-bound iron porphyrin (**PPSR-yne**, Scheme 1) involves an O−O bond heterolysis of an Fe^{III}−OOH species as the rate-determining step (RDS), the RDS of an imidazole-bound porphyrin (**PIM**, Scheme 1) is the O−O bond heterolysis of an Fe^{II}−OOH intermediate. In the case of thiolate axial ligand, a large H/D kinetic solvent isotope effect for both the $4e^-$ and $2e^-$ O_2 reduction is observed.

Scheme 1. Imidazole-Bound Complex PIM (1) and the Thiolate-Bound Complex PPSR-yne (2)

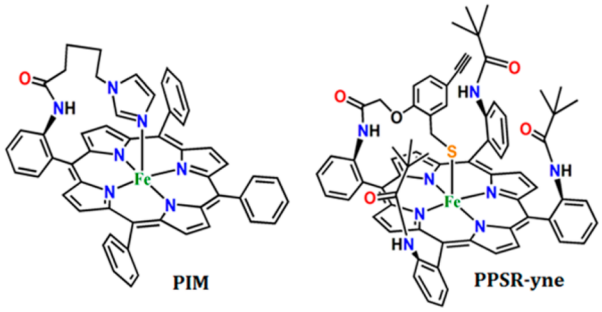

RESULTS AND ANALYSIS

Cyclic voltammetric (CV) experiments in pH 7 buffer with these Fe-porphyrin complexes, physiadsorbed on surfaces, show clear $Fe^{III/II}$ redox processes in the absence of oxygen (Figure S1A, Supporting Information). While the $Fe^{III/II}$ potential ($E_{1/2}$) is pH-dependent for PIM over pH 5−8 with a slope of 51 mV/pH, consistent with a $1e^-/1H^+$ PCET pathway, for PPSR-yne the redox potential is pH-dependent below pH 7 with a slope of 44 mV/pH and then becomes almost pH-independent (Figure S1B,C, Supporting Information).[74−76] In case of PPSR-yne, the CV data at different pH values indicate that the $E_{1/2}$ shows little pH dependence between pH 7−10 relative to PIM. This is consistent either with an RS-Fe^{III} ⇔ RS-Fe^{II} [both the systems present as five-coordinated high-spin (5C HS) species] or RS-Fe^{III}−OH_2 ⇔ RS-Fe^{II}−OH_2 [both the systems present as six-coordinated low-spin (6C LS) species] redox equilibrium in pH 7 buffer. The possibilities of the presence of either 5C Fe^{III} or 6C Fe^{III} under resting state can be delineated by SERRS-RDE data (vide infra). In the presence of oxygen, PIM shows oxygen reduction reaction (ORR) at potentials similar to formal $Fe^{III/II}$ potentials in pH 7, which implies that the potential determining step (PDS; defined as the most thermodynamically uphill step in the catalytic ORR cycle involving lowest reduction potential during ORR process)[77] of ORR for PIM involves the Fe^{III} to Fe^{II} reduction step (Figure 1A). Alternatively, for PPSR-yne, the catalyst

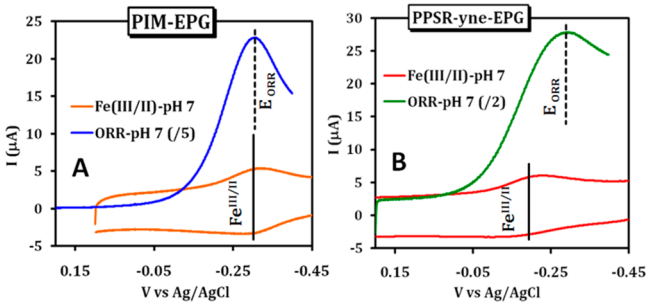

Figure 1. Overlay of CV (under anaerobic conditions) and LSV (under aerobic conditions) for (A) PIM and (B) PPSR-yne, respectively, on edge plane graphite surfaces.

shows ORR at potentials that are distinctly more negative than the formal $Fe^{III/II}$ potentials suggesting that the Fe^{III} to Fe^{II} reduction step is not the PDS in pH 7 (Figure 1B).

The electrocatalytic O_2 reduction is investigated using ring disc electrochemistry (RDE) technique, which not only helps in determining the number of electrons involved in ORR and catalytic rate constants evaluated from the Koutecky−Levich (K−L) equation, $I^{-1} = i_K^{-1} + i_L^{-1}$ (see Supporting Information for details), but also establishes the stability of these catalysts on the electrode surfaces.[78−80] From a linear plot (known as K−L plot) of I^{-1} obtained at multiple rotation rates versus the inverse square root of the angular rotation rate ($\omega^{-1/2}$), values of slopes are obtained at different potentials, which yields the number of electrons (n) delivered to the substrate during electrocatalytic ORR. The second-order rate of catalysis (k_{cat}) can also be evaluated from the intercept of this K−L plot (see Supporting Information for details). The chemical reaction that limits the current is assumed to be first order in O_2 since the limiting current (i_k) is found to be proportional to the O_2 concentration.[81−83] Both PIM and PPSR-yne, physiadsorbed on edge plane graphite (EPG), show a substrate diffusion limited catalytic O_2 reduction current below −0.25 V versus Ag/AgCl in pH 7 with the corresponding n values, which are very close or equal to 4 in each case, and k_{cat} values are obtained to be $2.3 \pm 0.26 \times 10^6$ M^{-1} s^{-1} and $1.1 \pm 2 \times 10^7$ M^{-1} s^{-1}, respectively (Figure S3, Supporting Information).[74,84] Similar RDE experiments in pD 7 buffer show values of n very close to 4 for both PIM and PPSR-yne, and k_{cat} values are estimated to be $2.2 \pm 0.34 \times 10^6$ M^{-1} $s^{-1}$and $0.61 \pm 0.07 \times 10^6$ M^{-1} s^{-1}, respectively (Figure 2).[85,86] Note that the LSVs of PPSR-yne in D_2O do not show a mass-transfer limited catalytic current even at large overpotentials. However, the exact reason behind this lack of saturation of ORR currents at various rotation rates is unclear at this point. The k_{cat} values obtained for PIM and PPSR-yne in H_2O and D_2O indicate the presence of a minor solvent KIE of 1.04 for PIM (Table 1) and a large solvent KIE, a lower limit (vide infra), of ∼18 for PPSR-yne. The KIE, in general, show the isotope effect of the RDS, which may inherently mask the isotope effects of other steps that are relatively much faster. Note that a K−L analysis could not be performed on C_8SH or $C_{16}SH$ self-assembled monolayer (SAM)-modified electrodes as the catalysts are unstable through the duration of the experiments.

DOI: 10.1021/ic5029959
Inorg. Chem. 2015, 54, 2383−2392

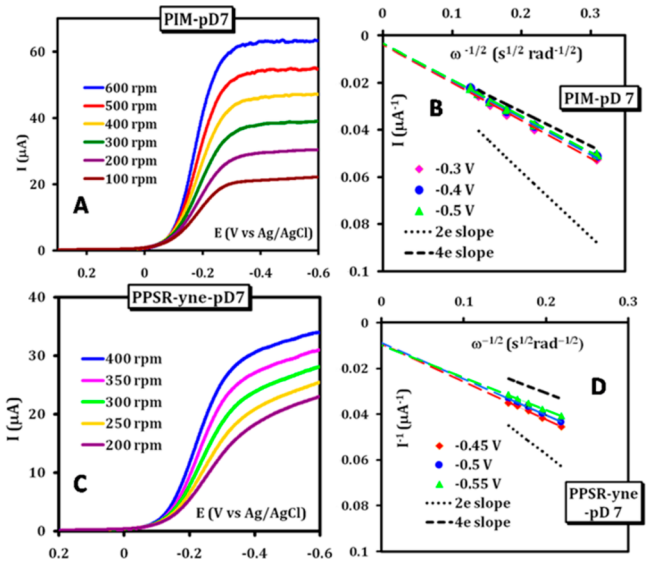

Figure 2. LSV of PIM (A) and PPSR-yne (C) physiadsorbed on EPG in pD 7 buffer at a scan rate of 50 mV/s at multiple rotations. (B) and (D) are the *K*–*L* plots of the respective catalysts at variable potentials. The theoretical plots for $2e^-$ and $4e^-$ processes are indicated by the black dotted and dashed lines, respectively.

The Tafel slopes for O_2 reduction under slow scan rates and at various rotation speeds have been found to be 119 mV/dec and 121 mV/dec in case of pH 7 buffer and 121 mV/dec and 123 mV/dec in case of pD 7 buffer for PIM and PPSR-yne on EPG, respectively (Figures S4 and S5, Supporting Information, and Table 1). ORR currents obtained upon physiadsorbing these catalysts on C_8SH SAM yield Tafel slopes of 134 and 126 mV/dec in pH 7 buffer and 136 and 126 mV/dec in pD 7 buffer for PIM and PPSR-yne, respectively (Figures S4 and S5 and Table 1). The slight increase in Tafel slope when physiadsorbed on C_8SH relative to when physiadsorbed on EPG suggests that the electron flux is slower through C_8SH SAM-modified Au electrodes relative to EPG. Since these values are close to 120 mV/dec, a $1e^-$ RDS in the kinetic regime is likely to be involved in ORR.[46,87] Thus, the RDS in the kinetic regime involves a single electron transfer for both these catalysts immobilized on both EPG and C_8SH SAM-modified electrodes. The fact that the PPSR-yne complex does not show a pure substrate diffusion limited current in D_2O at high overpotentials (Figure 2C) suggests that the k_{cat} value estimated in D_2O is approximately a lower limit.

The selectivity of this multielectron/multiproton ORR can be analyzed by measuring the amount of partially reduced oxygen species (PROS) produced, if any, during O_2 reduction using rotating ring disc electrochemistry (RRDE) technique (see Supporting Information for details). The PROS values in every case are calculated at a potential where the Pt ring current maximizes.[88,89] The data indicate that PIM produces 3.5 ± 1.0% PROS in H_2O and 0.8 ± 0.2% PROS in D_2O (Table 1). This indicates an isotope effect of 4.5 on the PROS production step for PIM. The selectivity of O_2 reduction has also been investigated in C_8SH and hexadecanethiol ($C_{16}SH$) SAM-covered Au electrodes where the electron-transfer (ET) rates are moderate ($\sim 1 \times 10^3$ s^{-1}) and very slow (6–10 s^{-1}), respectively, compared to the EPG surfaces (Figure 3 and

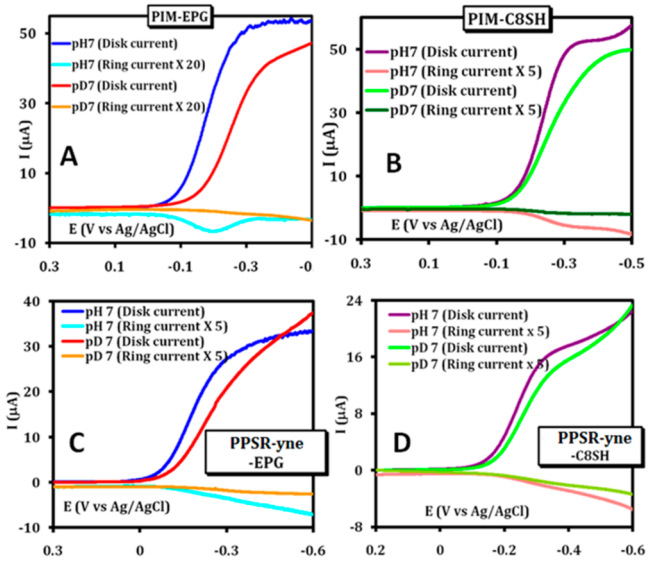

Figure 3. RRDE data of PIM (A and B) and PPSR-yne (C and D) in air saturated pH 7 and pD 7 buffers when physiadsorbed on EPG (A and C, respectively) and on C_8SH-modified Au electrode (B and D, respectively).

Figure S6, Supporting Information).[74] The amount of PROS produced by PIM and PPSR-yne at various ET rates, in both pH 7 and pD 7 (Table 1), increases with decreasing ET rate from the electrode to the catalyst. The values obtained for PIM show that the isotope effect on the amount of PROS is maximum in EPG (~4.5) and decreases to 2.5 and 2 in the cases of C_8SH and $C_{16}SH$ SAM-modified electrode, respectively (Table 1 and Figure S7A, Supporting Information). The data are suggestive of the fact that the PROS-producing step must be H/D isotope-sensitive irrespective of ET rate to the catalyst. In the case of PPSR-yne similar trend is observed but with smaller isotope effects (Table 1 and Figure S7B, Supporting Information).

The amount of PROS varies with the applied potential (i.e., the driving force for ORR). For PIM on EPG the PROS

Table 1. Extent of H/D Isotope Effect on Kinetic Parameters in EPG and Amount of PROS at Various ET Rate for PIM and PPSR-yne

		kinetics of ORR		PROS analyses (%)		
catalyst		k_{cat} (1×10^6) (M^{-1} s^{-1})	Tafel slope (mV/dec)	EPG	C_8SH	$C_{16}SH$
PIM	pH	2.3 ± 0.26	119 ± 2	3.5 ± 1.0	10 ± 0.5	16 ± 1.0
	pD	2.2 ± 0.34	121 ± 3	0.8 ± 0.2	4.1 ± 0.3	8 ± 0.9
	H/D	~1.04		4.5	2.5	2
PPSR-yne	pH	11.1 ± 2	121 ± 2	13.2 ± 0.2	15.5 ± 0.6	22.2 ± 2.1
	pD	0.61 ± 0.07	123 ± 5	5.1 ± 0.2	8.9 ± 1.1	20.1 ± 1.9
	H/D	>18		2.6	1.7	1.1

DOI: 10.1021/ic5029959
Inorg. Chem. 2015, 54, 2383–2392

current increases as the O_2 reduction current increases in the kinetic control region and after going through a maximum (Figure 3A, cyan) at −0.20 V versus Ag/AgCl, it diminishes gradually at lower potential, that is, in the potential region when the current becomes mass-transfer limited. Greater PROS in the kinetic regime relative to the mass-transfer limited region indicates that there is a direct competition between the $2e^-/2H^+$ reduction of O_2 (PROS) and $4e^-/4H^+$ reduction of O_2 (no PROS), and increasing the driving force favors the later process. It is consistent with the fact that the RDS for the $4e^-/4H^+$ reduction of O_2 in the kinetic region is likely to be an ET step. However, the RDS for $2e^-/2H^+$ step is not an ET step as in such a case the ring current ($2e^-/2H^+$) would not have decayed at high overpotential; rather, it would have saturated like the disk current ($4e^-/4H^+$). PPSR-yne, on EPG electrode, shows an opposite trend; that is, the $2e^-/2H^+$ current and the $4e^-/4H^+$ current increases with increasing driving force indicating that (a) the RDS of both the processes involve ET in the kinetic regime and (b) the rate of former is enhanced relative to the rate of latter on increasing the driving force (vide infra).[90]

PROS represent the ratio between the H_2O_2 current and the total catalytic current. In these cases where the catalytic current in mostly $4e^-/4H^+$ O_2 reduction (n = 4 in RDE), PROS represents approximately the rates of $2e^-/2H^+$ reduction and $4e^-/4H^+$ reduction currents (eq 1). Thus, calculating the KIE on the k_{cat} value of $4e^-/4H^+$ ORR (k_{4e}) and amount of PROS produced, one can roughly estimate the extent of KIE on the k_{cat} of $2e^-/2H^+$ ORR (k_{2e}) by considering the fact that the amount of PROS measured is the ratio of $2e^-/2H^+$ current (I_{cat}^{2e}) and total catalytic current (I_{cat}^{total}), where $I_{cat}^{total} \approx I_{cat}^{4e}$ (I_{cat}^{4e}, $4e^-/4H^+$ ORR current for the reduction/conversion of O_2 to H_2O only). Equation 1 can be reorganized to obtain eq 2 for the H/D isotope effects on the $2e^-/2H^+$ O_2 reduction rate.

$$\%\text{of PROS} = \frac{I_{cat}(2e^-)}{I_{cat}(4e^-)} \equiv \frac{k_{2e}}{k_{4e}} \quad (1)$$

$$\%\text{of PROS(H/D)} = \frac{k_{2e}(H)}{k_{4e}(H)} \times \frac{k_{4e}(D)}{k_{2e}(D)}$$

$$=> \frac{k_{2e}(H)}{k_{2e}(D)} = \%\text{of PROS(H/D)} \times \frac{k_{4e}(H)}{k_{4e}(D)} \quad (2)$$

Considering the above equations, KIE on k_{2e} were evaluated to be 4.7 and ∼47, for PIM and PPSR-yne, respectively, on EPG. Note that the $k_{2e}(H/D) \approx 47$ is a lower limit of the H/D KIE as $k_{4e} > 18$ for reasons discussed earlier. Thus, a combination of RDE and RRDE yields the H/D isotope effects on the RDS of the $2e^-/2H^+$ and $4e^-/4H^+$reduction of O_2 for imidazole- and thiolate-bound iron porphyrin catalysts immobilized on EPG electrodes.

Conventionally intermediates involved in O_2 reduction by an enzyme or a synthetic model are investigated during a single turnover reaction. Alternatively, these ORR mechanisms can also be investigated using SERRS-RDE when the system is under steady state where the species that accumulate under steady state can be identified and can help to identify the slowest step(s) in the catalytic cycle.[91] SERRS-RDE data of PIM in the oxidized condition in pH 7 show the presence of Fe^{III} HS species (Figure 4A).[74] In the presence of O_2, when the electrode is held at reducing potential where it is involved in steady state (i.e, at −0.5 V vs Ag/AgCl), the ν_2 band at 1565

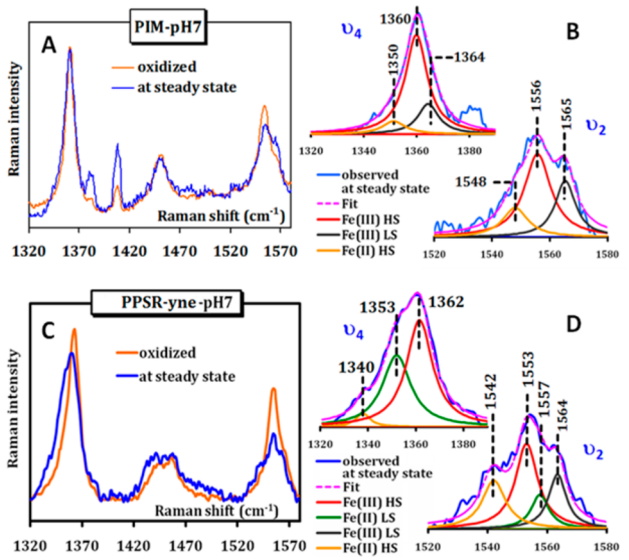

Figure 4. SERRS-RDE data of PIM (A and B) and PPSR-yne (C and D), physiadsorbed on C_8SH-modified Ag electrode, in the high-frequency region under oxidized (orange) (0 V vs Ag/AgCl) and steady-state (blue) (−0.5 V vs Ag/AgCl) conditions in air-saturated pH 7 buffer at 200 rpm rotation. The ν_4 and ν_2 bands of the steady-state spectra of the catalysts along with their Lorentzian fits showing different components are presented in B and D.

cm^{-1} corresponding to an Fe^{III} LS species is found to increase in intensity (Figure 4B) relative to the resting oxidized state. Along with the LS Fe^{III} species an Fe^{II} HS species having ν_4 and ν_2 bands at 1350 and 1548 cm^{-1}, respectively, grows in (Figure 4B).[73,92] The same species with almost similar intensities can be observed in D_2O under steady-state conditions having ν_2 bands at 1542 and 1565 cm^{-1} and ν_4 bands 1348 and 1363 cm^{-1} corresponding to Fe^{II} HS and Fe^{III} LS species, respectively (Figure 5A,B).[93] SERRS-RDE data of the PPSR-yne in pH 7 under resting state show the ν_4 band at 1363 cm^{-1}, 1354 cm^{-1} and the ν_2 band at 1555 cm^{-1}, 1559 cm^{-1} (Figure 4C) corresponding to an Fe^{III} HS and Fe^{II} LS species, respectively. Simultaneous Lorentzian fits of the ν_2 and ν_4 region of the data indicate the presence of a peak at 1567 cm^{-1} corresponding to LS Fe^{III} species. In the presence of O_2 in pH 7 buffer under steady-state conditions the ν_2 band at 1564 cm^{-1} corresponding to an Fe^{III} LS species is found to increase in intensity (Figure 4D). Along with the Fe^{III} species some Fe^{II} HS species as well as some Fe^{II} LS, corresponding to ν_4 bands at 1340 cm^{-1}, and 1353 cm^{-1} and ν_2 bands at 1542 cm^{-1}, and 1557 cm^{-1}, respectively, have been found to increase in intensity (Figure 4D). SERRS-RDE data in pD 7 buffer show the presence of the same species under steady-state conditions (Figure 5D,E). Interestingly the accumulation of LS Fe^{III} species (shown by black arrow in Figure 5F) is higher in D_2O buffer compared to H_2O buffer for PPSR-yne (vide infra) when a difference spectrum between H_2O and D_2O is being considered (Figure 5F). This is not the case for PIM (Figure 5C). The higher accumulation of LS species in D_2O for PPSR-yne implies an H/D isotope effect on the decay of the LS Fe^{III} species.

The electrochemical and SERRS-RDE data are consistent with distinct O_2 reduction mechanisms for the imidazole (PIM, Scheme 2) and thiolate (PPSR-yne, Scheme 3) ligated Fe-porphyrin complexes. The reduction of the resting Fe^{III} species (**i**, Scheme 2) in PIM follows a CPET pathway (step **1a**, Scheme 2), which should give rise to Fe^{II} HS (**ii**, Scheme 2)

DOI: 10.1021/ic5029959
Inorg. Chem. 2015, 54, 2383−2392

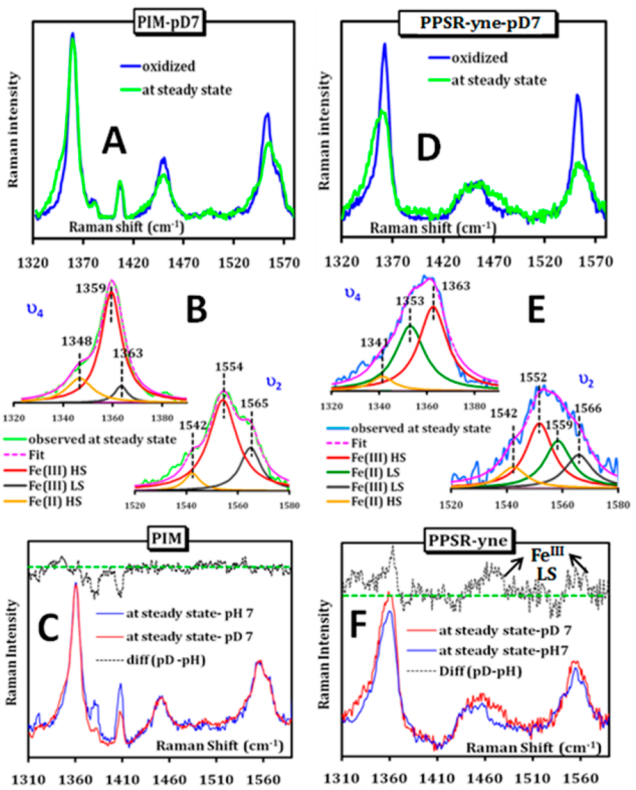

Figure 5. SERRS-RDE data of PIM (A and B) and PPSR-yne (D and E), physiadsorbed on C_8SH-modified Ag electrode, in the high-frequency region under oxidized (orange) (0 V vs Ag/AgCl) and steady-state (blue) (−0.5 V vs Ag/AgCl) conditions in air-saturated pD 7 buffer at 200 rpm rotation. The ν_4 and ν_2 bands of the steady-state spectra of the catalysts along with their Lorentzian fits showing different components are presented in B and E. Difference spectra of SERRS-RDE data of (C) PIM and (F) PPSR-yne physiadsorbed on C_8SH-modified Ag electrode (black dotted line), in the high-frequency region under steady-state conditions in air-saturated pD 7 (red) and pH 7 (blue) buffers.

Scheme 2. Proposed Mechanism of Oxygen Reduction by PIM Immobilized on Surface

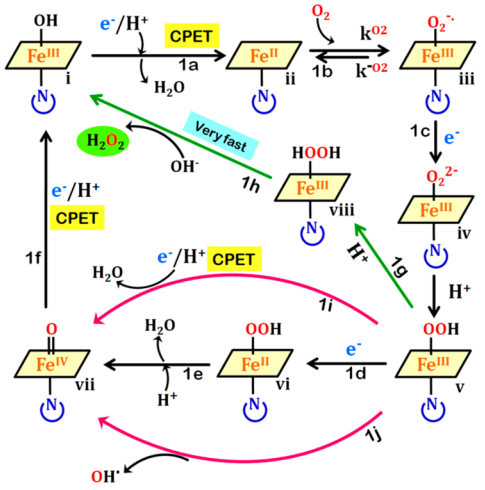

upon reduction. The k_{cat} value of ORR for PIM does not show significant H/D isotope effect in the mass-transfer limited region where the overall kinetics is determined by a step that does not involve ET. Thus, the steps **1a**, **1c**, **1d**, **1f**, and **1i** in

Scheme 3. Proposed Mechanism of Oxygen Reduction by PPSR-yne Immobilized on Surface

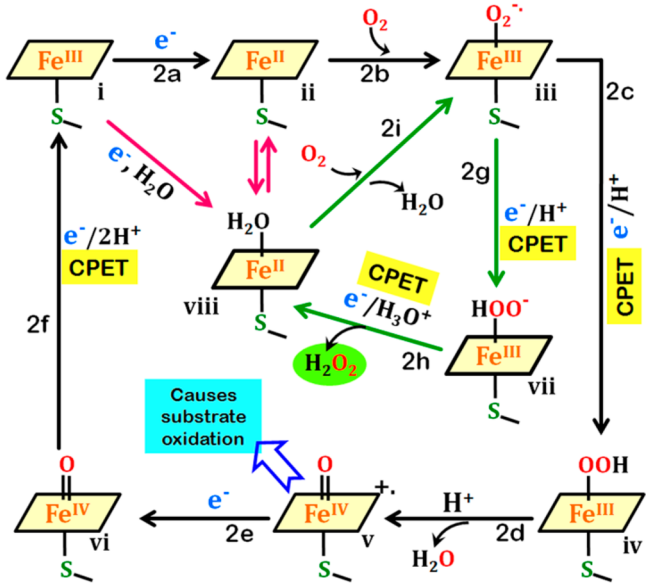

Scheme 2 cannot be the RDS in this region. The accumulation of an LS Fe^{III} species in the SERRS-RDE data at these potentials along with the absence of H/D isotope effect on the k_{cat} value suggest that either step **1j** or step **1e** is the RDS in the mass-transfer limited region. The homolysis of an imidazole-bound Fe^{III}−OOH species (step **1j**, Scheme 2) is calculated to have barriers of ∼20 kcal/mol.[94,95] Thus, this step is likely to have first-order rate of 0.02 s^{-1} (considering Eyring equation). The observed rate for PIM will include a pre-equilibrium constant of O_2 binding. This equilibrium constant of O_2 binding to other imidazole-bound Fe^{II} porphyrins (both proteins and models) is of the order of 1×10^2 to 1×10^1.[96,97] Factoring this into account, the first-order rate in the RDS is ∼5−50 s^{-1}, which is ∼1×10^3 times higher than the calculated value. Thus, the heterolytic cleavage of the Fe^{II}−OOH species (step **1e**) is likely to be the RDS for PIM. O_2 binding to imidazole-bound iron porphyrins (similar protein active sites and model complexes) has rate values > 1×10^7 M^{-1} s^{-1} and is thus unlikely to be the RDS.[97] Further considering the fact that the k_{cat} of PIM is an order of magnitude lower than that of PPSR-yne, for the O_2-binding rate (k_{O2}) in PIM to be the RDS, it must be slower than the k_{O2} for the thiolate-bound PPSR-yne. This is unlikely due to the stronger trans effect of the thiolate in PPSR-yne relative to imidazole in PIM.

The k_{cat} value, determined at different pH values, does not show significant pH dependences (Table S1, Supporting Information) implying that the pK_a of the Fe^{II}−OOH species is much greater than the pH range of investigation. The pK_a of an imidazole-bound Fe^{III}−OOH proximal oxygen is estimated to be 7.15 ± 0.05 here (vide infra, Figure 6A) and 5.35 ± 0.05 from modeling of CPET behavior of imidazole-bound heme.[98] It is suggested that reduction of the central metal can lead to an increase of 36 units in the pK_a of bound −OH ligands for iron systems.[99] Thus, it is quite likely that the pK_a of Fe^{II}−OOH species is >40, which is significantly higher than the pH range evaluated, and hence no pH dependence on k_{cat} is observed.

Protonation of the proximal O atom of the Fe^{III}−OOH species (**v**, Scheme 2) will produce Fe^{III}−H_2O_2 species (**viii**,

DOI: 10.1021/ic5029959
Inorg. Chem. 2015, 54, 2383−2392

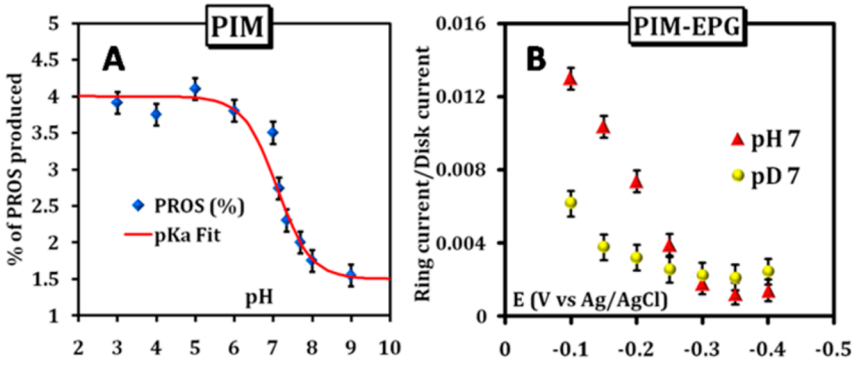

Figure 6. (A) Simulation of experimental points for the amount of PROS produced for PIM immobilized on EPG at different pH buffers (pK_a model fit). (B) Plot of the ratio of ring current to disc current vs the potential to the disc applied for PIM immobilized on EPG in both pH 7 and pD 7 buffers.

step **1g**, Scheme 2) that will release H_2O_2 in the solution to be detected in the Pt ring in the RRDE experiments. In fact a plot of amount of PROS detected at different pH values shows the presence of a single protonation equilibrium with a pK_a of (7.15 ± 0.05) (Figure 6A).[100] Such protonation steps, in the active site of heme and nonheme enzymes, are associated with reasonable H/D kinetic isotope effects (~2−4.2)[50,101,102] consistent with the isotope effect of 4.7 observed for the PROS production step here. The plot of the ratio of the ring current to the disk current with the applied potential in both pH 7 and pD 7 buffers (Figure 6B) show that the ratio decreases as the potential is lowered (i.e., as the driving force for ET is increased) suggesting that the species (**viii**, Scheme 2) responsible for generation of H_2O_2 is depleted at higher driving force by a competitive ET step in the ORR cycle. This is consistent with the proposed mechanism as the rate of $2e^-/2H^+$ reduction depends on proton concentration (Figure 6A), and the rate of $4e^-/4H^+$ reduction depends on the rate of ET rate and will increase with increase in driving force; that is, step **1d** will dominate step **1g** at lower applied potentials leading to the observed decrease in PROS. Thus, the step responsible for PROS production in imidazole-bound iron porphyrin is the protonation of the proximal oxygen atom of an Fe^{III}−OOH species, which has a pK_a value of 7.15.

On the basis of the assimilated electrochemical and spectroscopic data, an ORR catalytic cycle can also be proposed (Scheme 3) for PPSR-yne complex. The electrochemical data suggest that in the mass-transfer limited region there is a KIE >18 on k_{cat}. Therefore, the steps **2c**, **2e**, **2f**, **2g**, and **2h** in Scheme 3 cannot be the RDS in this mass-transfer limited region; rather, the protonation of an LS Fe^{III}−OOH species (**iv**, Scheme 3) is likely to be the RDS in this region. The observation of LS Fe^{III} species and its higher population in D_2O in the SERRS-RDE data during steady state (Figure 5F) is consistent with this proposal. The $2e^-/2H^+$ O_2 reduction step shows an isotope effect >47. Further a plot of the ratio of $2e^-/2H^+$ and $4e^-/4H^+$ current (Figure 7) indicates that the $2e^-$ current increases monotonously with increasing driving force even at high overpotentials in H_2O where the $4e^-$ current is mass-transfer limited. The monotonous increase in the $2e^-$ current with increase in applied overpotential is limited in D_2O relative to H_2O reflecting the large KIE on the $2e^-/2H^+$ reduction current (Figure 3C,D). This is also reflected in the ratio of the $2e^-/2H^+$ and $4e^-/4H^+$ currents, which does not increase significantly in D_2O as it does in H_2O (Figure 7). Both of the above facts (i.e., the increase in $2e^-/2H^+$ current with

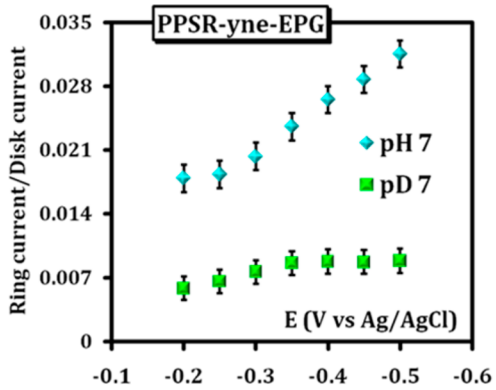

Figure 7. Plot of the ratio of ring current to disc current vs the potential to the disc applied for PPSR-yne in both pH 7 and pD 7 buffers.

applied overpotential and the large H/D KIE) suggest that the step resulting in $2e^-/2H^+$ oxygen reduction is CPET. Protonation of proximal oxygen of an Fe^{III}−O_2^- species (**iii**, Scheme 3), formed upon binding of oxygen to Fe^{II} (steps **2b** and **2i**, Scheme 3), can be a CPET step resulting in an Fe^{III}−$(HO)O^-$ species (**vii**, Scheme 3), which has the neutral oxygen of the hydroperoxide anion bound to Fe^{III}, and is thus prone to hydrolysis. The hydrolysis of the above species will result in production of H_2O_2 (step **2h**, Scheme 3), the $2e^-/2H^+$ reduction product of O_2, which is detected in the Pt ring. The greater KIE in the CPET to the proximal oxygen relative to the distal oxygen is likely due to a greater barrier in transferring a proton (likely from the solvent) and an electron simultaneously to the sterically protected bound proximal O atom relative to the unbound distal O atom.

Our past investigation of analogous thiolate-bound iron porphyrin complexes indicated that, while the resting Fe^{III} species exists mainly in the 5C HS state in these complexes, the reduced species is a mixture of 5C HS and 6C LS states.[74] It has also been observed that the LS Fe^{II} state is associated with weaker O_2 binding kinetics compared to its HS analogue. Thus, we believe, in this case, the accumulation of an LS Fe^{II} species along with the LS Fe^{III} species in the SERRS-RDE data for PPSR-yne under steady state is observed for the aforesaid reason.

DOI: 10.1021/ic5029959
Inorg. Chem. 2015, 54, 2383−2392

DISCUSSION

A combination of RDE, RRDE, and SERRS-RDE experiments on thiolate- and imidazole-bound iron porphyrin complexes indicate that axial ligands can lead to distinct RDS involved in O_2 reduction. In the imidazole-bound complex the rate-determining step in the $4e^-/4H^+$ O_2 reduction pathway does not show H/D isotope effect, but the protonation of an LS Fe^{III}−OOH species, involved in the $2e^-/2H^+$ O_2 reduction, shows an isotope effect of 4.7. Alternatively, for a thiolate-bound iron porphyrin complex, while the RDS of the $2e^-/2H^+$ process involves a CPET step having KIE > 47, the RDS for the $4e^-/4H^+$ process is a protonation having KIE > 18. The push effect of the thiolate manifests itself by increasing the electron density at the iron center raising the pK_a of the Fe^{III}−OOH species enough to cause facile protonation and O−O bond cleavage so that an approximate first-order rate of $[1 \times 10^7 \times (2.2 \times 10^{-4})] \approx 2.2 \times 10^3\ s^{-1}$ (where $[O_2] = 2.2 \times 10^{-4}$ M) can be attained in the mass-transfer limited region during $4e^-/4H^+$ reduction of O_2. However, in the case of the imidazole-bound species the pK_a of this species is low, and it does not undergo fast O−O cleavage. Rather, it must be reduced to Fe^{II}−OOH before the O−O bond can be cleaved in the RDS of O_2 reduction in the mass-transfer limited region with the first-order rate of $[(2.3 \times 10^6) \times (2.2 \times 10^{-4})] \approx 500\ s^{-1}$. In the kinetic region, where the ET from the electrode is slow, the Fe^{III}−OOH produces PROS via protonation of the proximal oxygen of $pK_a = 7.15$.

In the thiolate-bound PPSR-yne, where the high pK_a of the O_2-derived axial ligands induces fast CPET steps in ORR circumventing slow pure ET steps in the mechanism of imidazole-bound PIM, the selectivity of O_2 reduction is determined by the site of proton transfer to the bound superoxide species. The proximal oxygen, which is bound to the iron in the porphyrin ring, is difficult to access by the proton donor solvent relative to the distal oxygen. Thus, the donor−acceptor distance in the CPET transition state (TS) is likely to be higher in the former case resulting in larger KIE. Note that, in the case of nonheme iron system, Fukuzumi's group has recently shown an inverse KIE to be present where the formation of O−H bond is coupled with electron transfer in a nonheme Fe^{IV}=O species in the presence of a strong acid in an organic solvent.[60] Protonation of the distal O atom leads to O−O bond cleavage ($4e^-/4H^+$ reduction), whereas the protonation of the proximal O atom leads to H_2O_2 production. Conceivably, a similar situation may be encountered in the active site of thiolate-bound O_2-activating cyt P450. However, specific hydrogen-bonding interaction between the distal O atom ensures protonation at the distal atom minimizing formation of H_2O_2, that is, uncoupling reaction.[103] The organized second sphere interaction in the distal site of cyt P450 not only directs the site of protonation but also lowers the activation barrier for protonation. The rate of O−O bond cleavage is facile in the biological enzyme active sites having rate greater than $1 \times 10^4\ s^{-1}$ due to well-positioned distal amino acid residues. This rate is much higher than the O−O bond cleavage of PPSR-yne, which does not have an organized distal structure for proton transfer to the distal oxygen.[104,105] The first protonation step in the cyt P450 is reported to have an isotope effect of 1.8 in the wild-type enzyme.[50] However, mutating the Asp 251 residue (Asp 251 is the proposed source of proton transfer to the iron-bound hydroperoxide species) results in the increase of a solvent isotope effect of 10.[106,107] Thus, the lack of any organization in the distal structure of PPSR-yne may be the reason for this high solvent KIE of the protonation step.

The SERRS-RDE technique allows a direct look into the catalytic cycles of the catalysts, supplementing the information obtained from the electrochemical analysis alone. Applications of this technique allow probing the rate-determining steps in the mass-transfer region directly. The oxidation and spin-state marker bands and their intensity redistribution in H_2O/D_2O proved to be helpful in identifying the mechanism of ORR.

EXPERIMENTAL DETAILS

Materials. All reagents were of the highest grade commercially available and were used without further purification. Octanethiol (C_8SH), hexadecanethiol ($C_{16}SH$), potassium hexafluorophosphate (KPF_6), deuterium oxide (D_2O), and the solvents used were purchased from Sigma-Aldrich. Disodium hydrogen phosphate dihydrate ($Na_2HPO_4{\cdot}2H_2O$), buffer capsules, and potassium chloride (KCl) were purchased from Merck. Au wafers were purchased from Platypus Technologies (1000 Å of Au on 50 Å of Ti adhesion layer on top of a Si(III) surface). EPG electrodes and Au discs for the RRDE experiments and Ag discs for SERRS and SERRS-RDE experiments were purchased from Pine Instruments, USA. The catalysts *meso*-mono[*o*-5-(*N*-imidazolyl)valeramidophenyl]-triphenylporphyrinatoiron(III)bromide (PIM) and clickable P450 (PPSR-yne) (Scheme 1) were prepared following procedures given in literature reports.[84,108]

Instrumentation. All electrochemical experiments were performed using a CH Instruments (model CHI710D) Electrochemical Analyzer. Biopotentiostat, reference electrodes, and Teflon plate material evaluating cell (ALS Japan) were purchased from CH Instruments. The RRDE setup from Pine Research Instrumentation (E6 series ChangeDisc tips with AFE6M rotor) was used to obtain the RRDE data. SERRs data were collected using a Trivista 555 spectrograph (Princeton Instruments) and using 413.1 nm excitation from a Kr^+ laser (Coherent, Sabre Innova SBRC-DBW-K).

Construction of the Electrodes. *Physiabsorption of the Catalysts on Edge Plane Graphite.* Catalyst (60 μL) from a 1 mM solution of the respective catalysts in chloroform ($CHCl_3$) is deposited on a freshly cleaned EPG electrode mounted on RRDE setup. After the evaporation of the solvent, the surface is thoroughly dried with N_2 gas and sonicated in ethanol. Finally before using it for electrochemical experiments, the modified electrodes are washed with triply distilled water.

Formation of Self-Assembled Monolayer. Au wafers and discs are cleaned electrochemically by sweeping several times between 1.5 and −0.3 V vs Ag/AgCl in 0.5 M H_2SO_4. Ag discs are cleaned in alumina (size: 1, 0.3, and 0.05 μ) and then roughened in 0.1 M KCl solution as described in literature.[109] SAM solutions are prepared using the concentration of the thiols as reported in our previous work.[74] Freshly cleaned Au wafers and discs and freshly roughened Ag discs are rinsed with triply distilled water and ethanol, purged with N_2 gas, and immersed in the depositing solution for ∼8 h.

Physiabsorption of the Catalysts onto the Self-Assembled Monolayer. Au wafers and discs and roughened Ag discs immersed in the deposition solution are taken out before experiments and rinsed with ethanol followed by triply distilled deionized water and then dried with N_2 gas. The wafers are then inserted into a Plate Material Evaluating Cell (ALS Japan), and the discs were mounted on a platinum ring disc assembly (Pine Instruments, USA). These SAM-modified surfaces are immersed in the $CHCl_3$ solution of the catalyst for ∼30 min and are then rinsed with chloroform, ethanol, and triply distilled water followed by drying with N_2 gas before the electrochemical and SERRS-RDE experiments.

Cyclic Voltammetry Experiments. All CV experiments are done in pH 7 buffer (unless otherwise mentioned) containing 100 mM $Na_2HPO_4{\cdot}2H_2O$ and 100 mM KPF_6 (supporting electrolyte) using Pt wire as the counter electrode and Ag/AgCl as the reference electrode.

DOI: 10.1021/ic5029959
Inorg. Chem. 2015, 54, 2383−2392

Solvent Kinetic Isotope Effect. The KIE was studied by generating the RDE and PROS in deuterated buffer (pD 7) and normal protonated buffer (pH 7). Deuterated buffer (pD 7) was prepared by dissolving pH 7 buffer capsule in D_2O, and the pH of the resulting solution was measured by pH meter to be 6.6. To obtain the exact pD value, 0.4 should be added to the pH meter reading.[110,111] Since the pK_a of the protonable groups shift by about the same value, the protonation level of these groups is about the same in H_2O and D_2O, respectively, at the same pH meter reading.[110,111]

Coverage Calculation. The coverage for a particular species is estimated by integrating the oxidation and reduction currents of the respective species.[74,112]

Partially Reduced Oxygen Species. Both the platinum ring and the Au disc are polished by alumina powder (grit sizes: 1, 0.3, and 0.05 μ), electrochemically cleaned, and inserted into the RRDE tip, which is then mounted on the rotor and immersed into a cylindrical glass cell equipped with Ag/AgCl reference and Pt counter electrodes. The collection efficiency (CE) of the RRDE setup is measured in a 2 mM $K_3Fe(CN)_6$ and 0.1 M KNO_3 solution at 10 mV/s scan rate and 300 rpm rotation speed. A 20 ± 2% CE is generally recorded during these experiments. The potential at which the ring is held during the collection experiments at pH 7 for detecting H_2O_2 was obtained from literature.[113] For normal measurement of PROS the ratio of the disk and ring currents are taken at the potential where the Pt ring maximizes during RRDE experiments.

Surface-Enhanced Resonance Raman Spectroscopy Coupled with Rotating Disc Electrochemistry. Ag discs are cleaned using Alumina powder (grit sizes 1, 0.3, and 0.05 μm), roughened in 0.1 M KCl solution using reported procedures,[109,114] and then immersed in SAM solutions. The roughened modified Ag discs are then inserted into the RRDE setup for the collection of SERRS data.[115,116] Catalysts are physiadsorbed in a similar manner as described in the previous section. Experiments were done using an excitation wavelength of 413.1 nm, and the power used at the electrode surface is ∼10−12 mW. While collecting the spectra at resting/oxidized state the disc was held at 0 and at −0.5 V vs Ag/AgCl to obtain a spectrum during steady-state O_2 reduction. The electrode is rotated at constant speed of 200 rpm in either case.[73]

■ ASSOCIATED CONTENT

Supporting Information

Additional notes on RDE and RRDE, CV data, *K*−*L* plot analyses, Tafel slopes for PIM and PPSR-yne, RRDE data of PIM and PSSR-yne, production of PROS by PIM and PSSR-yne expressed as a percentage, SERRS data of PIM, determination of k_{cat} for PIM in different pH, additional references. This material is available free of charge via the Internet at http://pubs.acs.org.

■ AUTHOR INFORMATION

Corresponding Author

*E-mail: icad@iacs.res.in.

Notes

The authors declare no competing financial interest.

■ ACKNOWLEDGMENTS

The authors sincerely acknowledge Department of Science and Technology, Grant Nos. DST/SR/IC-35-2009 and SB/S1/IC-25/2013 for funding this work. S.C., K.S., and P.K.D. acknowledge CSIR for senior research fellowships. S.S. acknowledges Int. Ph.D. program of IACS. We acknowledge the reviewers for their constructive criticism.

■ REFERENCES

(1) Su, Q.; Klinman, J. P. *Biochemistry* **1998**, *37*, 12513−12525.
(2) Chang, C. J.; Chang, M. C. Y.; Damrauer, N. H.; Nocera, D. G. *Biochim. Biophys. Acta, Bioenerg.* **2004**, *1655*, 13−28.
(3) Rosenthal, J.; Nocera, D. G. *Acc. Chem. Res.* **2007**, *40*, 543−553.
(4) Kaila, V. R. I.; Verkhovsky, M. I.; Wikstrom, M. *Chem. Rev.* **2010**, *110*, 7062−7081.
(5) Siegbahn, P. E. M.; Blomberg, M. R. A. *Chem. Rev.* **2010**, *110*, 7040−7061.
(6) Weinberg, D. R.; Gagliardi, C. J.; Hull, J. F.; Murphy, C. F.; Kent, C. A.; Westlake, B. C.; Paul, A.; Ess, D. H.; McCafferty, D. G.; Meyer, T. J. *Chem. Rev.* **2012**, *112*, 4016−4093.
(7) Reece, S. Y.; Nocera, D. G. *Annu. Rev. Biochem.* **2009**, *78*, 673−699.
(8) Barry, B. A. *Nat. Chem.* **2014**, *6*, 376−377.
(9) Mitchell, P. *Nature* **1961**, *191*, 144−8.
(10) Born, M.; Oppenheimer, R. *Ann. Phys.* **1927**, *84*, 457−84.
(11) Weissbluth, M. *Atoms and Molecules;* Academic: New York, 1978.
(12) Bell, R. P. *The Tunnel Effect on Chemistry;* Chapman and Hall: London, U.K., 1980.
(13) Bell, R. P. *Chem. Soc. Rev.* **1974**, *3*, 513−544.
(14) Migliore, A.; Polizzi, N. F.; Therien, M. J.; Beratan, D. N. *Chem. Rev.* **2014**, *114*, 3381−3465.
(15) Cong, Z.; Kinemuchi, H.; Kurahashi, T.; Fujii, H. *Inorg. Chem.* **2014**, *53*, 10632−10641.
(16) Fukuzumi, S.; Kobayashi, T.; Suenobu, T. *J. Am. Chem. Soc.* **2010**, *132*, 1496−1497.
(17) Cha, Y.; Murray, C. J.; Klinman, J. P. *Science* **1989**, *243*, 1325−30.
(18) Mayer, J. M.; Rhile, I. J. *Biochim. Biophys. Acta, Bioenerg.* **2004**, *1655*, 51−58.
(19) Warren, J. J.; Tronic, T. A.; Mayer, J. M. *Chem. Rev.* **2010**, *110*, 6961−7001.
(20) Siegbahn, P. E. M.; Blomberg, M. R. A. *Chem. Rev.* **2010**, *110*, 7040−7061.
(21) Miller, A.-F.; Padmakumar, K.; Sorkin, D. L.; Karapetian, A.; Vance, C. K. *J. Inorg. Biochem.* **2003**, *93*, 71−83.
(22) Reece, S. Y.; Seyedsayamdost, M. R.; Stubbe, J.; Nocera, D. G. *J. Am. Chem. Soc.* **2007**, *129*, 8500−8509.
(23) Reece, S. Y.; Lutterman, D. A.; Seyedsayamdost, M. R.; Stubbe, J.; Nocera, D. G. *Biochemistry* **2009**, *48*, 5832−5838.
(24) Pizano, A. A.; Lutterman, D. A.; Holder, P. G.; Teets, T. S.; Stubbe, J.; Nocera, D. G. *Proc. Natl. Acad. Sci. U. S. A.* **2012**, *109* (39−43), S39/1−S39/8.
(25) Davydov, R.; Osborne, R. L.; Kim, S. H.; Dawson, J. H.; Hoffman, B. M. *Biochemistry* **2008**, *47*, 5147−5155.
(26) Li, F.; England, J.; Que, L. *J. Am. Chem. Soc.* **2010**, *132*, 2134−2135.
(27) Meyer, T. J.; Huynh, M. H. V.; Thorp, H. H. *Angew. Chem., Int. Ed.* **2007**, *46*, 5284−5304.
(28) Lyon, E. J.; Shima, S.; Buurman, G.; Chowdhuri, S.; Batschauer, A.; Steinbach, K.; Thauer, R. K. *Eur. J. Biochem.* **2004**, *271*, 195−204.
(29) Shiota, Y.; Juhasz, G.; Yoshizawa, K. *Inorg. Chem.* **2013**, *52*, 7907−7917.
(30) Baik, M.-H.; Gherman, B. F.; Friesner, R. A.; Lippard, S. J. *J. Am. Chem. Soc.* **2002**, *124*, 14608−14615.
(31) Saito, K.; Rutherford, A. W.; Ishikita, H. *Proc. Natl. Acad. Sci. U. S. A.* **2013**, *110* (954−959), S954/1−S954/4.
(32) Nicolet, Y.; Lemon, B. J.; Fontecilla-Camps, J. C.; Peters, J. W. *Trends Biochem. Sci.* **2000**, *25*, 138−143.
(33) Chang, C. J.; Loh, Z.-H.; Shi, C.; Anson, F. C.; Nocera, D. G. *J. Am. Chem. Soc.* **2004**, *126*, 10013−10020.
(34) Madhiri, N.; Finklea, H. O. *Langmuir* **2006**, *22*, 10643−10651.
(35) Costentin, C. *Chem. Rev.* **2008**, *108*, 2145−2179.
(36) Heinze, K.; Marano, G.; Fischer, A. *J. Inorg. Biochem.* **2008**, *102*, 1199−1211.
(37) Costentin, C.; Robert, M.; Saveant, J.-M.; Teillout, A.-L. *Proc. Natl. Acad. Sci. U. S. A.* **2009**, *106* (11829−11836), S11829/1−S11829/5.

DOI: 10.1021/ic5029959
Inorg. Chem. 2015, 54, 2383−2392

(38) Costentin, C.; Robert, M.; Saveant, J.-M.; Teillout, A.-L. *ChemPhysChem* **2009**, *10*, 191−198.
(39) Hammes-Schiffer, S. *Acc. Chem. Res.* **2009**, *42*, 1881−1889.
(40) Hatay, I.; Su, B.; Li, F.; Mendez, M. A.; Khoury, T.; Gros, C. P.; Barbe, J.-M.; Ersoz, M.; Samec, Z.; Girault, H. H. *J. Am. Chem. Soc.* **2009**, *131*, 13453−13459.
(41) Lee, J. Y.; Lee, Y.-M.; Kotani, H.; Nam, W.; Fukuzumi, S. *Chem. Commun.* **2009**, 704−706.
(42) Trammell, S. A.; Lebedev, N. *J. Electroanal. Chem.* **2009**, *632*, 127−132.
(43) Zhang, W.; Rosendahl, S. M.; Burgess, I. J. *J. Phys. Chem. C* **2010**, *114*, 2738−2745.
(44) Albers, A.; Demeshko, S.; Dechert, S.; Saouma, C. T.; Mayer, J. M.; Meyer, F. *J. Am. Chem. Soc.* **2014**, *136*, 3946−3954.
(45) Samanta, S.; Mittra, K.; Sengupta, K.; Chatterjee, S.; Dey, A. *Inorg. Chem.* **2013**, *52*, 1443−1453.
(46) Mittra, K.; Chatterjee, S.; Samanta, S.; Dey, A. *Inorg. Chem.* **2013**, *52*, 14317−14325.
(47) Matson, B. D.; Carver, C. T.; Von Ruden, A.; Yang, J. Y.; Raugei, S.; Mayer, J. M. *Chem. Commun.* **2012**, *48*, 11100−11102.
(48) Gelb, M. H.; Heimbrook, D. C.; Malkonen, P.; Sligar, S. G. *Biochemistry* **1982**, *21*, 370−7.
(49) Cha, Y.; Murray, C. J.; Klinman, J. P. *Science* **1989**, *243*, 1325−30.
(50) Aikens, J.; Sligar, S. G. *J. Am. Chem. Soc.* **1994**, *116*, 1143−4.
(51) Nesheim, J. C.; Lipscomb, J. D. *Biochemistry* **1996**, *35*, 10240−10247.
(52) Rickert, K. W.; Klinman, J. P. *Biochemistry* **1999**, *38*, 12218−12228.
(53) Huynh, M. H. V.; Meyer, T. J. *Angew. Chem., Int. Ed.* **2002**, *41*, 1395−1398.
(54) Chen, Z.; Vannucci, A. K.; Concepcion, J. J.; Jurss, J. W.; Meyer, T. J. *Proc. Natl. Acad. Sci. U. S. A.* **2011**, *108* (E1461-E1469), SE1461/1−SE1461/12.
(55) Gregory, M. C.; Denisov, I. G.; Grinkova, Y. V.; Khatri, Y.; Sligar, S. G. *J. Am. Chem. Soc.* **2013**, *135*, 16245−16247.
(56) Damrauer, N. H.; Hodgkiss, J. M.; Rosenthal, J.; Nocera, D. G. *J. Phys. Chem. B* **2004**, *108*, 6315−6321.
(57) Young, E. R.; Rosenthal, J.; Hodgkiss, J. M.; Nocera, D. G. *J. Am. Chem. Soc.* **2009**, *131*, 7678−7684.
(58) Huynh, M.-H. V.; White, P. S.; Meyer, T. J. *Angew. Chem., Int. Ed.* **2000**, *39*, 4101−4104.
(59) Huynh, M. H. V.; Meyer, T. J.; White, P. S. *J. Am. Chem. Soc.* **1999**, *121*, 4530−4531.
(60) Park, J.; Morimoto, Y.; Lee, Y.-M.; Nam, W.; Fukuzumi, S. *Inorg. Chem.* **2014**, *53*, 3618−3628.
(61) Nam, W. *Acc. Chem. Res.* **2007**, *40*, 522−531.
(62) Oh, N. Y.; Suh, Y.; Park, M. J.; Seo, M. S.; Kim, J.; Nam, W. *Angew. Chem., Int. Ed.* **2005**, *44*, 4235−4239.
(63) Rosenthal, J.; Nocera, D. G. *Acc. Chem. Res.* **2007**, *40*, 543−553.
(64) Makris, T. M.; von Koenig, K.; Schlichting, I.; Sligar, S. G. *Biochemistry* **2007**, *46*, 14129−14140.
(65) Bistolas, N.; Wollenberger, U.; Jung, C.; Scheller, F. W. *Biosens. Bioelectron.* **2005**, *20*, 2408−2423.
(66) Fruk, L.; Kuo, C.-H.; Torres, E.; Niemeyer, C. M. *Angew. Chem., Int. Ed.* **2009**, *48*, 1550−1574.
(67) Ramanavicius, A.; Ramanaviciene, A. *Fuel Cells* **2009**, *9*, 25−36.
(68) Onoda, A.; Kakikura, Y.; Hayashi, T. *Dalton Trans.* **2013**, *42*, 16102−16107.
(69) Sengupta, K.; Chatterjee, S.; Mukherjee, S.; Dey, S. G.; Dey, A. *Chem. Commun.* **2014**, *50*, 3806−3809.
(70) Gewirth, A. A.; Thorum, M. S. *Inorg. Chem.* **2010**, *49*, 3557−3566.
(71) Samanta, S.; Sengupta, K.; Mittra, K.; Bandyopadhyay, S.; Dey, A. *Chem. Commun.* **2012**, *48*, 7631−7633.
(72) Sengupta, K.; Chatterjee, S.; Samanta, S.; Bandyopadhyay, S.; Dey, A. *Inorg. Chem.* **2013**, *52*, 2000−2014.
(73) Sengupta, K.; Chatterjee, S.; Samanta, S.; Dey, A. *Proc. Natl. Acad. Sci. U. S. A.* **2013**, *110*, 8431−8436.
(74) Chatterjee, S.; Sengupta, K.; Samanta, S.; Das, P. K.; Dey, A. *Inorg. Chem.* **2013**, *52*, 9897−9907.
(75) PIM has a tendency to form μ-oxo dimer at higher pH (beyond pH 8). The $E_{1/2}$ values were evaluated separately on fresh surfaces for every pH to avoid any confusion of dimerization. In pH 7, PIM remains as hydroxide bound six-coordinated monomeric species (see Supporting Information, Figure S8, for further details).
(76) The reason behind the 44 mV/pH slope of $E_{1/2}$ below pH 7 for PPSR-yne is similar to that of PIM, which has also an open distal side and may have similar origins. However, note that PPSR-yne remains as thiolate-bound complex in pH 7, where all the mechanistic investigations were performed (see refs 74 and 84).
(77) Note that this PDS may not reflect the $Fe^{III/II}$ redox step.
(78) Bard, A. J.; Faulkner, L. R. *Eleectrochemical Methods;* J. Wiley: New York, 1980; p 300.
(79) Wilhelm, E.; Battino, R.; Wilcock, R. J. *Chem. Rev.* **1977**, *77*, 219−262.
(80) Saveant, J.-M. *Elements of Molecular and Biomolecular Electrochemistry;* Wiley-Interscience: Hoboken, NJ, 2006.
(81) Kobayashi, N.; Nishiyama, Y. *J. Phys. Chem.* **1985**, *89*, 1167−1170.
(82) Durand, R. R.; Bencosme, C. S.; Collman, J. P.; Anson, F. C. *J. Am. Chem. Soc.* **1983**, *105*, 2710−2718.
(83) The i_k value differs by a factor 2.35 when concentration of O_2 dissolved in pH 7 has been increased by 2.3 (Figure S2, Supporting Information).
(84) Samanta, S.; Das, P. K.; Chatterjee, S.; Sengupta, K.; Mondal, B.; Dey, A. *Inorg. Chem.* **2013**, *52*, 12963−12971.
(85) Before every experiment, the surface coverages of the catalyst were calculated from their respective Fe^{III}/Fe^{II} CV currents obtained in deoxygenated pH 7 buffer. These coverages vary (though slightly) in each experiment and therefore are taken into account to estimate the k_{cat} for that particular experiment.
(86) The k_{cat} values were evaluated from the intercepts of the $K-L$ plots obtained at different potentials in the diffusion-limited region. The intercepts vary with overpotentials, as may be expected, and therefore are taken into account for evaluating k_{cat} in each case.
(87) Tse, E. C. M.; Schilter, D.; Gray, D. L.; Rauchfuss, T. B.; Gewirth, A. A. *Inorg. Chem.* **2014**, *53*, 8505−8516.
(88) Boulatov, R.; Collman, J. P.; Shiryaeva, I. M.; Sunderland, C. J. *J. Am. Chem. Soc.* **2002**, *124*, 11923−11935.
(89) For those RRDE data that lack the maxima in the Pt ring current, PROS was calculated at such potential where the disk current maximizes.
(90) On a slower ET surface (C_8SH) the effect of increasing the driving force is negligible for either of these catalysts.
(91) Sengupta, K.; Chatterjee, S.; Samanta, S.; Dey, A. *Proc. Natl. Acad. Sci. U.S.A.* **2013**, *110*, 8431−8436.
(92) Burke, J. M.; Kincaid, J. R.; Peters, S.; Gagne, R. R.; Collman, J. P.; Spiro, T. G. *J. Am. Chem. Soc.* **1978**, *100*, 6083−6088.
(93) Since the band intensities in resonance Raman are only qualitative, and not quantitative, the exact ratios of the species accumulated on the electrode surface cannot be assigned accurately for H_2O/D_2O experiments.
(94) Vidossich, P.; Fiorin, G.; Alfonso-Prieto, M.; Derat, E.; Shaik, S.; Rovira, C. *J. Phys. Chem. B* **2010**, *114*, 5161−5169.
(95) Chen, H.; Hirao, H.; Derat, E.; Schlichting, I.; Shaik, S. *J. Phys. Chem. B* **2008**, *112*, 9490−9500.
(96) Niederhoffer, E. C.; Timmons, J. H.; Martell, A. E. *Chem. Rev.* **1984**, *84*, 137−203.
(97) Collman, J. P.; Brauman, J. I.; Iverson, B. L.; Sessler, J. L.; Morris, R. M.; Gibson, Q. H. *J. Am. Chem. Soc.* **1983**, *105*, 3052−3064.
(98) Mukherjee, S.; Bandyopadhyay, S.; Chatterjee, S.; Dey, A. *Chem. Commun.* **2014**, *50*, 12304−12307.
(99) Han, W.-G.; Lovell, T.; Noodleman, L. *Inorg. Chem.* **2002**, *41*, 205−218.
(100) The pK_a of 7.15 eliminates the possibility of an $Fe^{III}-O_2^-$ species as the base since pK_a of free superoxide is 4.89, and metal binding should reduce the pK_a.

DOI: 10.1021/ic5029959
Inorg. Chem. 2015, 54, 2383−2392

(101) Emerson, J. P.; Coulter, E. D.; Cabelli, D. E.; Phillips, R. S.; Kurtz, D. M., Jr. *Biochemistry* **2002**, *41*, 4348−4357.
(102) Huang, V. W.; Emerson, J. P.; Kurtz, D. M., Jr. *Biochemistry* **2007**, *46*, 11342−11351.
(103) Dey, A.; Jiang, Y.; Ortiz de Montellano, P.; Hodgson, K. O.; Hedman, B.; Solomon, E. I. *J. Am. Chem. Soc.* **2009**, *131*, 7869−7878.
(104) Roth, J. P.; Cramer, C. J. *J. Am. Chem. Soc.* **2008**, *130*, 7802−7803.
(105) Shintaku, M.; Matsuura, K.; Yoshioka, S.; Takahashi, S.; Ishimori, K.; Morishima, I. *J. Biol. Chem.* **2005**, *280*, 40934−40938.
(106) Vidakovic, M.; Sligar, S. G.; Li, H.; Poulos, T. L. *Biochemistry* **1998**, *37*, 9211−9219.
(107) Gerber, N. C.; Sligar, S. G. *J. Am. Chem. Soc.* **1992**, *114*, 8742−8743.
(108) Das, P. K.; Chatterjee, S.; Samanta, S.; Dey, A. *Inorg. Chem.* **2012**, *51*, 10704−10714.
(109) Bulovas, A.; Talaikyte, Z.; Niaura, G.; Kazemekaite, M.; Marcinkeviciene, L.; Bachmatova, I.; Meskys, R.; Razumas, V. *Chemija* **2007**, *18*, 9−15.
(110) Glasoe, P. K.; Long, F. A. *J. Phys. Chem.* **1960**, *64*, 188−90.
(111) Chowen, K. B.; Schowen, R. L. *Methods Enzymol.* **1982**, *87*, 551−606.
(112) Collman, J. P.; Devaraj, N. K.; Eberspacher, T. P. A.; Chidsey, C. E. D. *Langmuir* **2006**, *22*, 2457−2464.
(113) Zhang, Y.; Wilson, G. S. *J. Electroanal. Chem.* **1993**, *345*, 253−71.
(114) Hildebrandt, P.; Macor, K. A.; Czernuszewicz, R. S. *J. Raman Spectrosc.* **1988**, *19*, 65−69.
(115) Murgida, D. H.; Hildebrandt, P. *Chem. Soc. Rev.* **2008**, *37*, 937−945.
(116) Sharma, B.; Frontiera, R. R.; Henry, A.-I.; Ringe, E.; Van Duyne, R. P. *Mater. Today* **2012**, *15*, 16−25.

DOI: 10.1021/ic5029959
Inorg. Chem. 2015, 54, 2383−2392